

RESEARCH ARTICLE


 OPEN ACCESS

Received: 09-06-2020

Accepted: 14-07-2020

Published: 31-07-2020

Editor: Dr. Natarajan Gajendran

Citation: Agdad A, Chaik M, Samba Vall CM, Abounachit O, Nkhaili L, kissani AE, Ait Dads H, Narjis A, Outzourhit A (2020) Structural, optical and electrical properties of Aluminum doped ZnO, CuO and their heterojunction fabricated using spin coating and Rf-Sputtering techniques. Indian Journal of Science and Technology 13(27): 2786-2796. <https://doi.org/10.17485/IJST/v13i27.674>

* Corresponding author.

M Chaik

Laboratory of Nanomaterials, Energy and Environment (LNEE), Faculty of Sciences Semlalia, Cadi Ayyad University, PO Box: 2390, Marrakech, 40000, Morocco. Tel.: +212658369094 cheikhmohamed5@gmail.com

Funding: None

Competing Interests: None

Copyright: © 2020 Agdad, Chaik, Samba Vall, Abounachit, Nkhaili, kissani, Ait Dads, Narjis, Outzourhit. This is an open access article distributed under the terms of the [Creative Commons Attribution License](https://creativecommons.org/licenses/by/4.0/), which permits unrestricted use, distribution, and reproduction in any medium, provided the original author and source are credited.

Published By Indian Society for Education and Environment ([ISSEE](https://www.indjst.org/))

Structural, optical and electrical properties of Aluminum doped ZnO, CuO and their heterojunction fabricated using spin coating and Rf-Sputtering techniques

A Agdad¹, M Chaik^{1*}, C M Samba Vall², O Abounachit³, L Nkhaili¹, A.El kissani¹, H Ait Dads¹, A Narjis¹, A Outzourhit¹

¹ Laboratory of Nanomaterials, Energy and Environment (LNEE), Faculty of Sciences Semlalia, Cadi Ayyad University, PO Box: 2390, Marrakech, 40000, Morocco. Tel.: +212658369094

² Laboratory of Renewable Energy and Environment, Faculty of Science Kenitra, Ibn Tofail University, POBox 133, Kenitra, Morocco

³ LP2M2E, Laboratory of Process, Metrology and Materials for Energy and Environment, Faculty of Sciences and techniques Gueliz, Cadi Ayyad University, BP 549, Marrakech, Morocco

Abstract

Objectives: The aim of this work is to fabricate and analyze the Aluminum Doped ZnO, Copper Oxide CuO and their heterojunction CuO/ZnO:Al using Spin Coating and Rf-Sputtering techniques. **Methods:** ZnO:Al was synthesized from a sol-gel precursor and deposited on Indium Tin Oxide-coated glass substrate ITO using spin coating. CuO thin films, on the other hand, were elaborated by RF-sputtering. The characterization of both thin films was performed by means of X-ray diffraction, scanning electron microscopy and UV-visible-NIR double beam spectrophotometer. The CuO/ZnO:Al heterojunction was fabricated and characterized using current voltage, capacitance-voltage and conductance-voltage measurements. **Findings:** The collected results confirm the rectifying nature of the junction with a built-in voltage V_{bi} of about 1.6 V.

Keywords: Copper oxide; Aluminum doped Zinc oxide; RF sputtering; spin coating; heterojunction

1 Introduction

Copper oxide CuO is a p-type semiconductor with a direct optical band-gap (E_g) between 1.51 and 1.74 eV⁽¹⁾. It has a high absorption coefficient, which makes it suitable as an absorber in solar cells and in photo-thermal energy conversion. The CuO is also widely applied in optoelectronic devices such as thin film transistors^(1,2). This material is very promising in these applications because of its low cost being earth abundant, environmental friendly and nontoxic. Up to now, thin films of CuO have been deposited by various techniques, such as reactive sputtering⁽³⁾, metal-organic chemical vapor deposition⁽⁴⁾ and electrochemical deposition^{(5),(6)}. On the other hand, aluminum doped zinc oxide ZnO:Al (AZO) is an n-type semiconductor with a direct optical band gap of about 3.3 eV⁽⁷⁾, which makes it useful as a transparent electron collecting (hole blocking) oxide. The conductivity of ZnO, and consequently its collection efficiency

of electrons, can be increased by doping⁽⁸⁾. Nowadays, among several kinds of transparent conductive oxides (TCO), ZnO:Al meets the requirements for contacting thin-film solar cells^(9–11). This is due to its abundance in nature, low cost and non-toxicity. In addition, ZnO:Al has been used in different applications such as gas sensors⁽¹²⁾, flat screen displays, touch panels and energy-saving windows^(13–18). High-quality AZO films are recently deposited by various processes such as spray pyrolysis⁽¹⁹⁾, chemical vapor deposition (CVD)⁽²⁰⁾, sol-gel process⁽²¹⁾, pulsed laser deposition⁽²²⁾, chemical spray⁽²³⁾, plasma enhanced CVD⁽²⁴⁾ and sputtering techniques^(25–27). The ZnO/CuO heterojunction where the oxides layers were prepared by various techniques have been reported in previous works^(28–30). Terasako et al. studied a heterojunction where the ZnO and CuO layers were both deposited by the chemical bath deposition (CDB) technique⁽³¹⁾. The authors reported a built-in voltage (V_{bi}) between 0.2 and 1.5 V for these heterostructures. On the other hand, Kumar et al.⁽³²⁾ fabricated CuO-composite/ZnO nanowire heterostructures and found a built-in voltage of 0.47 V. More recently, CuO-Cu₂O/ZnO:Al heterojunctions were developed by Hoppe et al. for selective volatile organic compound detection⁽³³⁾. The ZnO:Al films were deposited by a wet chemical method, while the mixed-phase CuO-Cu₂O was fabricated by first depositing a Cu layer on the ZnO:Al film by thermal evaporation followed by annealing in an air atmosphere at 425 °C⁽³³⁾. However, such high temperature treatment may degrade the interface between the two oxides (inter-diffusion) which, therefore will affect the quality of the heterojunction. Furthermore, a p-CuO/n-ZnO heterojunction was fabricated recently using the sol-gel spin-coating technique by Prabhu et al.⁽³⁴⁾. Their devices exhibited a rectification behavior with a turn on voltage of 2.5 V, and an ideality factor of more than 40 at high voltages⁽³⁴⁾. Solution processing of the CuO/ZnO heterojunction may affect the quality of the interface between the two oxides and hence the electrical properties of the junction. Vacuum processing of the junction, through reactive RF-sputtering of CuO on pre-fabricated and cleaned ZnO films may minimize such problems and also allow to control the oxide structure and stoichiometric easily. In our previous work, we based only on Rf-sputtering technique to fabricate CuO/ZnO heterojunction⁽³⁵⁾. In this work, we proposed to synthesize CuO and Aluminum doped ZnO thin films by the two different techniques RF-sputtering and spin coating respectively. These films were subsequently used to fabricate CuO/ZnO:Al heterojunction. In order to investigate the effect of doping ZnO by Aluminum and also the use of the two last deposition techniques, we studied the structural and optical properties of the elaborated films, and finally the electrical characteristics of the CuO/ ZnO:Al heterojunctions were measured and discussed.

2 Experimental Details

To prepare ZnO:Al thin films, the starting material was synthesized by sol-gel process. We used the zinc acetate 2-hydrate ($Zn(CH_3COO)_2 \cdot 2H_2O$) (99.5% purity) as a source of zinc. The absolute ethanol was used as a solvent and monoethanolamine (MEA) as a sol stabilizer. Aluminum was added as a dopant in the form of $(Al(NO_3)_3 \cdot 9H_2O)$ (extra purity) with an Al/Zn ratio of 1 %. A 0.5 M ethanolic solution of zinc acetate was prepared by dissolving 0.5 mole of zinc acetate 2-hydrate in 100 ml of the absolute ethanol in a conical flask. After vigorously stirring for 30 min, MEA was added drop-wise while stirring. The molar ratio of MEA/ Zn^{2+} was fixed at 1. The solution became clear after stirring for about 2 hours. ZnO:Al (1% of Al) film were deposited on bare glass, ITO and silicon (100) substrates by spin coating with spinning speed of 2000 rpm for 25 s. The thickness of the obtained ZnO film is on the order of 380 nm. CuO thin film was prepared by reactive RF-sputtering on glass substrate at room temperature from a pure Cu target (99.99 %) with a diameter of 10 cm. The reactive sputtering was carried out in an Ar/O₂ gas mixture containing 30 % of O₂. We deposited the thin film at an RF power of 200 W for a duration of 120 min which gives 590 nm film thickness. Each one of these grown films was subjected to electrical measurements.

The CuO/ZnO:Al/ITO/glass heterojunctions were prepared by first depositing ZnO:Al on ITO/glass using spin-coating and subsequently depositing CuO on the ZnO:Al/ITO/glass by reactive RF-sputtering. The structure is completed by depositing top Al circular electrodes (1mm of diameter) by thermal evaporation at $2 \cdot 10^{-5}$ mbar base pressure. The thickness of this Al layer is about 100 nm.

The structural properties of the various thin films previously developed, were investigated by XRD with an X-pert MPD diffractometer using the $Cu(K\alpha)$ radiation. Their surface morphology were studied by a TESCAN VEGA3 Scanning Electron Microscope (SEM). Optical transmittance measurements were carried out by using a Shimadzu UV-PC double-beam spectrophotometer in the range of 200–2000 nm.

The current-voltage (I-V) characteristics of Al/CuO/ZnO:Al/ITO/glass device were measured at room temperature using computer-controlled Keithley 410 programmable ammeter and voltmeter. The impedance measurements were performed by a Keithley LCZ3000 impedance meter.

3 Results and Discussion

3.1 Structural properties

Figure 1 shows the XRD patterns of typical ZnO:Al and CuO thin films singly deposited on glass substrates. For the ZnO:Al films (Figure 1-a), all peaks are assigned to the ZnO wurtzite phase (reference: JCPDS No.79-2205). No characteristic peaks of aluminum oxide or of any impurities were observed. In addition, no preferred growth direction is observed compared to the thin films deposited by RF-sputtering which exhibited a (100) preferred orientation on glass substrates as reported elsewhere⁽³⁵⁾.

The XRD patterns of CuO thin films deposited on glass substrate at 200 W and 30 % of O₂ are shown in Figure 1-b. The inset of Figure 1-b depicts the deconvolution of the peaks located at 35° and 75° using the Lorentzian line shapes. The peaks centered at 32.23°, 35.34°, 35.63°, 38.32°, 57.86°, 74.71° and 75.36° correspond respectively to the (110) , (002), (-111) , (111), (202), (004) and (-113) lattice planes of the monoclinic CuO phase with C2/c space group. These results are supported by the JCPDS No 80-0076 reference. In addition, the XRD spectrum is dominated by the intense peak attributed to the (002) lattice plane of the CuO monoclinic phase. No peaks attributed to Cu₂O or Cu₄O₃ phases are observed, which further confirms that the CuO phase is more stable under oxygen rich atmospheres⁽³⁶⁾,⁽³⁷⁾.

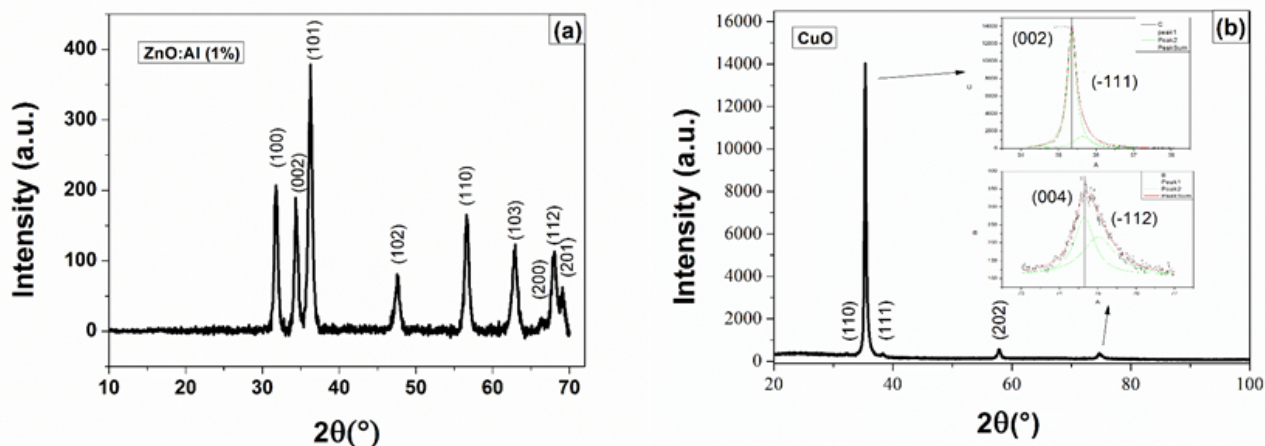


Fig 1. XRD pattern of (a)ZnO:Al and (b) CuO thin films deposited on glass substrates (The insets of figure 1-b shows the deconvolution of the peaks)

The lattice constants of the ZnO:Al films were calculated from the d-spacing of (hkl) planes of the quadratic phases through the following equation⁽³⁸⁾:

$$\frac{1}{d_{hkl}^2} = \frac{4}{3} \left[\frac{h^2 + hk + k^2}{a^2} \right] + \frac{l^2}{c^2} \quad ; \text{ with } \frac{c}{a} = \sqrt{3} \tag{1}$$

where d_(hkl) is the d-spacing of a given set of (hkl) planes, a and c are the lattice constants. The obtained parameters, listed in Table 1, are in good agreement with the known lattice parameters of ZnO⁽³⁹⁾. On the other hand, the parameters of CuO thin films, were calculated from the d-spacing of the monoclinic phase given in the literature work⁽⁴⁰⁾:

$$\frac{1}{d_{hkl}^2} = \left(\frac{h^2}{a^2} + \frac{l^2}{c^2} - \frac{2hl}{ac} \cos\beta \right) \frac{1}{\sin^2\beta} + \frac{k^2}{b^2} \tag{2}$$

where a, b, c and β were the lattice parameters.

The obtained lattice parameters for the CuO thin films are summarized in Table 1 . It is noticed that these parameters are in close agreement with previous reported values⁽¹¹⁾,⁽³⁵⁾. In addition, the crystallite size D of the films was determined from the Debye Scherrer equation given by⁽⁴¹⁾:

Table 1. Extracted parameters of the ZnO:Al and CuO thin films.

Thin film	Lattice parameters (Å)	grain size Dhkl (nm)
CuO $\beta=99.26^\circ$	a=4.718 b=3.457 c=5.141	20.4
ZnO:Al	a=3.248 c=5.207 c/a=1.603	15.0

$$\beta_{hkl} \cos \theta = \frac{K\lambda}{D} \tag{3}$$

where K is a constant which is approximately 0.9 while λ is the wavelength of the X-rays, β_{hkl} is the Full-Width at Half-Maximum intensity (FWHM) of the peak and θ is the corresponding Bragg angle. All the structural parameters of the ZnO:Al and CuO thin films are regrouped in the Table 1. The crystallite size for the ZnO:Al films are consistent with those reported for thin films prepared by spin-coating^{(11), (38)}.

Figure 2 -a shows a typical SEM surface image of the prepared ZnO:Al thin films. This SEM image reveals a homogeneous and smooth surface with no pin holes. The shown morphology is similar to that observed by Chavan et al.⁽⁴²⁾. The SEM image of CuO thin film, shown in Figure 2-b, reveals a homogeneous surface and well-distributed nano-sized grains⁽⁴³⁾. These characteristics are critical for obtaining good hetero-junctions (no short circuits in electrical measurement).

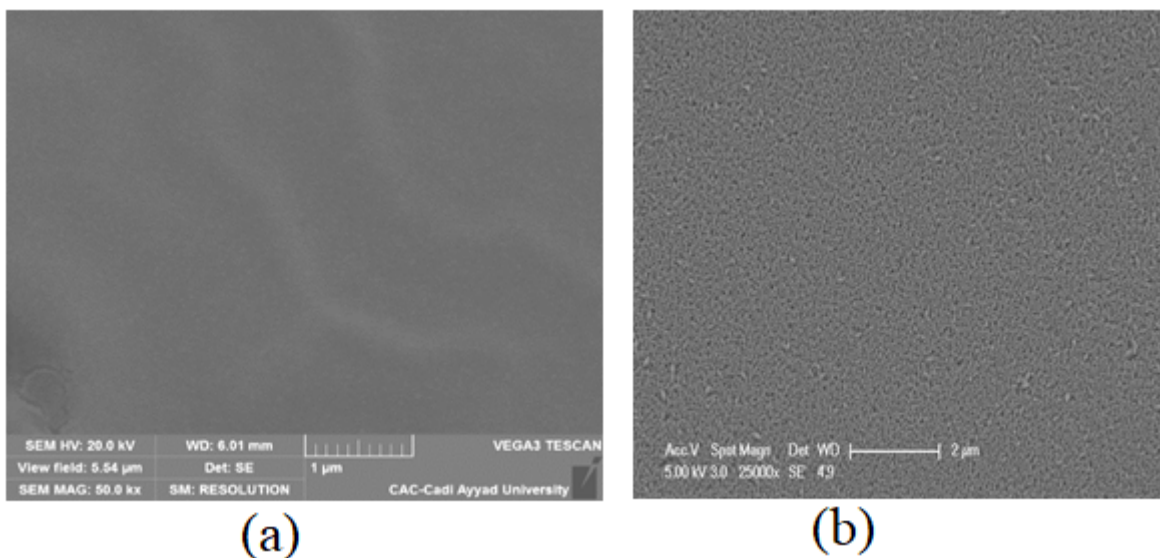


Fig 2. SEM image of (a) the ZnO:Al thin film developed by spin-coating method (b) CuO thin film deposited by RF sputtering.

3.2 Optical properties

Figure 3 shows the optical transmittance spectrum of the as-deposited ZnO and CuO thin films in 200-2000 nm wavelength range. The ZnO films are highly transparent in the visible range of the electromagnetic spectrum with an average transmittance value of 84 %. On the other hand, the CuO films are absorbing in the visible range. Their transmittance spectrum in the near IR region is marked by an average transmission of about 50% and also by the presence of interference fringes. These are an indication of the good quality and the smoothness of the surface in the films as observed in the SEM image.

The optical band gap of the thin films was determined from the variations of the absorption coefficient (α) with photon energy $h\nu$. The former parameter was calculated from the transmission spectra in the region where the film is absorbing through the relationship:

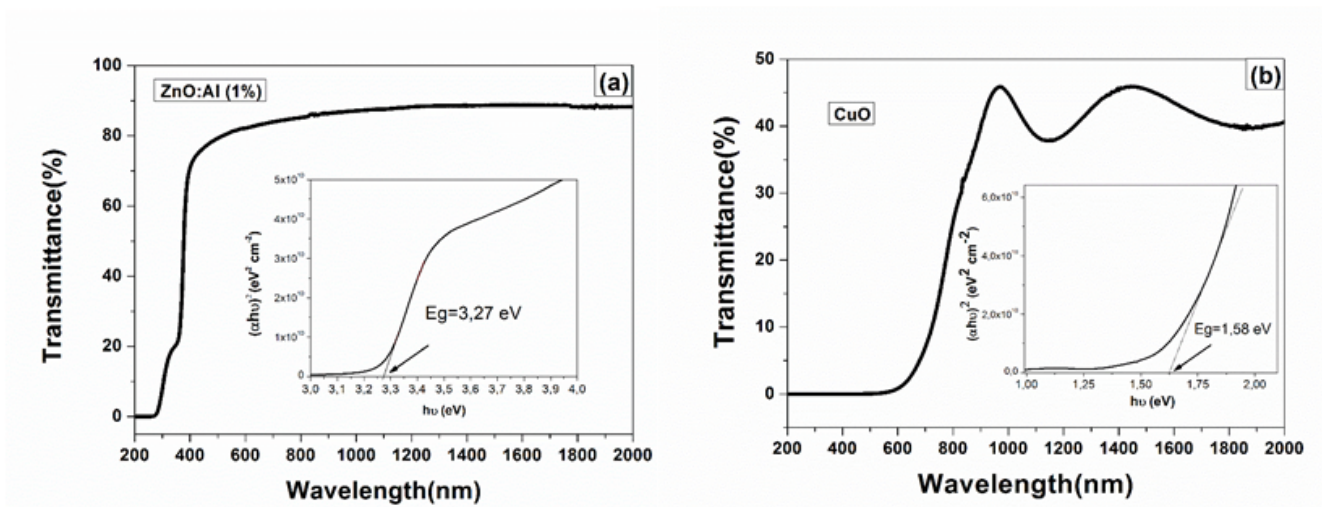


Fig 3. Optical transmission spectrum of (a) ZnO:Al thin film and (b) CuO thin film. Insets show the $(\alpha h\nu)^2$ versus photon energy $(h\nu)$

$$\alpha = -1/d \ln (1/T) \tag{4}$$

where d is the film thickness.

For photon energies above the band gap, the absorption coefficient is usually written in the form:

$$(\alpha h\nu)^{1/r} = k(h\nu - E_g) \tag{5}$$

with $r=1/2$ for direct allowed transitions, $r=3/2$ for direct forbidden transitions, $r=2$ for indirect allowed transitions and $r=3$ for indirect forbidden transitions.

Since both ZnO and CuO are direct band-gap semiconductors, the optical band-gap of these films can be determined from the linear part of the $(\alpha h\nu)^2$ vs $h\nu$ graphs (insets of Figure 3)⁽⁴⁴⁾. Other details concerning the determination of the optical parameters from the optical transmission spectrum were reported by Laaziz et al.⁽⁴⁵⁾. The optical gap of ZnO thin films was found to be 3.27 eV, which is in agreement with the reported value ($E_g = 3.28$ eV)^{(35), (46), (47)}. On the other hand, the optical band gap of CuO is found to be 1.58 eV, which is also consistent with previously reported values for CuO^{(35), (48)}.

In order to determine the refractive index of our samples, as presented in the transmittance spectra of samples, there are no, or small interference fringes. In this case, we used the Cauchy equation, which is valid for the thin film model⁽⁴⁹⁾:

$$n = n_{IR} + \frac{b}{\lambda} \quad , \quad b = \frac{NpZe^2}{4\pi\epsilon_0mC^2} \tag{6}$$

where n_{IR} is the refractive index in the infrared region, b is a constant, the constant b, n_{IR} , which can be determined from the transmittance spectra and used for extrapolation of all the wavelengths^(50,51).

It can be observed in Figure 4 that the refractive index of CuO thin film is decreasing with increasing wavelength, and in the order of 1.8^(50,51).

The variation of refractive index of ZnO:Al thin films from Cauchy's method too is shown in Figure 4. It was clear from Figure 4; the refractive index of the films decreased as the wavelength increased. The same phenomena is observed by A. M. Alsaad et al.^(52,53).

This refractive index of ZnO:Al (1.98) is greater than that of CuO thin film making ZnO:Al thin film an antireflective layer in hetero junction solar cell⁽⁵³⁾.

Using the relation of the absorption coefficient (α), the extinction coefficient (k) can be directly evaluated.

$$K = \frac{\alpha\lambda}{4\pi} \tag{7}$$

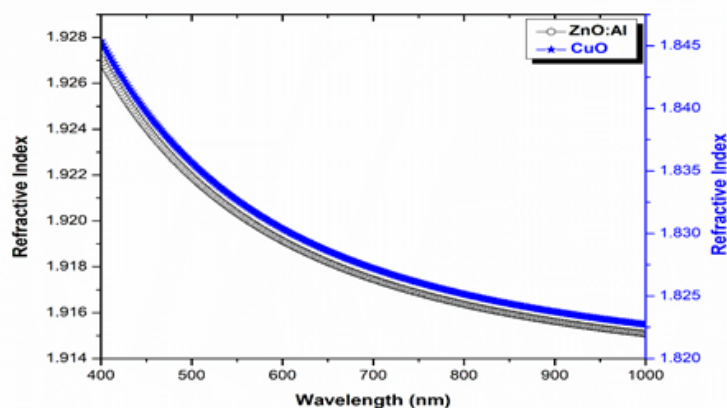


Fig 4. The variation refractive index of (a) the CuO and (b) the ZnO:Al thin films

The variation of extinction coefficient with wavelength for both ZnO:Al and CuO thin films are depicted in Figure 5. As can be seen in (Figure 5) the extinction coefficient increase with the increasing wavelength the maximum value of the extinction coefficient is at the edge of absorption⁽⁵⁴⁾. The highest extinction coefficient occurs for CuO thin film. This might be attributed to the better crystallite size, which enhances reduced the grain boundaries. In addition, the greater thickness could have led to an increase in optical scattering, which would have increased the value of the extinction coefficient.

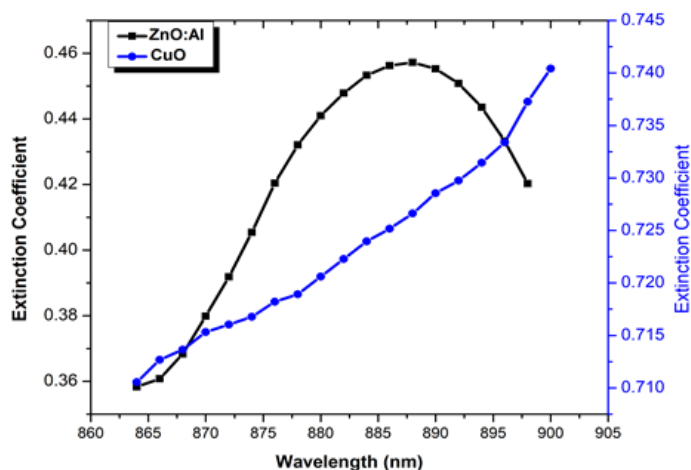


Fig 5. Extinction coefficient of ZnO:Al and CuO thin film

3.3 Zn O:Al/CuO heterojunction

The Current-Voltage (I-V) characteristic of a typical ZnO:Al/CuO hetero-junction fabricated by using the deposition techniques described above is shown in Figure 6. The characteristics are not linear, asymmetric and exhibit a rectifying behavior as the reverse bias current is much lower than the forward bias one. The turn-on voltage is about 0.6 V which is small compared to 2.5 V reported by Prabhu et al.⁽³⁴⁾ for heterojunctions based on the sol gel method.

The rectification ratio at ± 1 V, $I(+1V)/I(-1V)$ is on the order of 12 which is higher than that observed by other authors^(34,55). These parameters further support the good quality of the heterojunctions prepared by the present method.

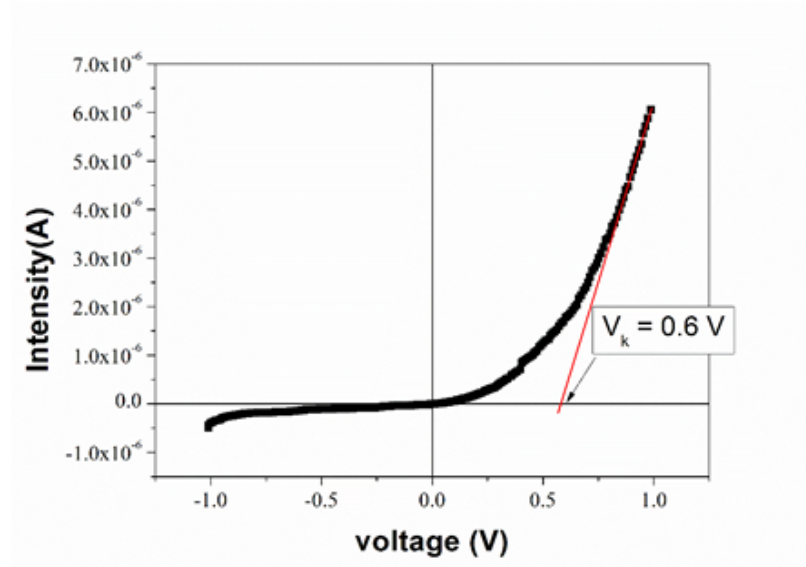


Fig 6. Current-Voltage characteristics of ITO/ ZnO:Al(1%)/CuO/Al device

As in the case of p-n junctions, the dark I-V characteristics of heterojunctions are usually described by the well-known modified Shockley equation⁽⁵⁶⁾ given by:

$$I = I_{sat} \left(\exp \left(\frac{V - R_s I}{nKT} \right) - 1 \right) + \frac{V - IR_s}{R_{sh}} \tag{8}$$

where I_{sat} is the saturation current,
 e is the electron charge,
 R_s is the series resistance,
 n is the ideality factor of the diode,
 k is the Boltzmann constant,
 T is the absolute temperature and
 R_{sh} is the shunt resistance.

The parameters R_{sh} and R_s were determined by the dynamic resistance method⁽⁴¹⁾ as described below. From equation 11, the dynamic resistance $R_d = dV / dI$ of the diode is given by following expression:

$$R_d = \frac{dV}{dI} = R_s + \frac{1}{\beta I_{sat} \exp^{\beta(V - IR_s)} + \frac{1}{R_{sh}}} \tag{9}$$

with $\beta = \frac{e}{nkT}$.

In the high-voltage region, where the effect of R_{sh} is negligible, $\beta I_{sat} \exp^{\beta(V - IR_s)} \gg \frac{1}{R_{sh}}$ and equation (12) becomes:

$$R_d = \frac{dV}{dI} \approx R_s + \frac{1}{\beta I_{sat} \exp^{\beta(V - IR_s)}} \approx R_s + \frac{1}{\beta I} \tag{10}$$

Therefore, in this region, R_d depends linearly on $1/I$. The slope of this line enables to calculate $\beta(n)$ and its y-intercept yields directly the series resistance R_s . On the other hand, in the low-voltage region, where $I_{sat} \exp^{\beta(V - IR_s)} \ll \frac{1}{R_{sh}}$, R_d tends asymptotically towards R_{sh} , which is supposed to be much higher than R_s .

The dynamic resistance (R_d), obtained from the results of Figure 6 by numerical differentiation is plotted against $1/I$ in Figure 7 -a. As expected, and according to the above arguments, two regions A and B can be clearly distinguished in this figure. In region B corresponding to the low-voltage region of the I-V characteristics, R_d is practically constant. This latter region gives

a shunt resistance R_{sh} of $3.5 \times 10^7 \Omega$. In the zone A shown with more details in Figure 7-b, the linear fit yields a series resistance R_s of $11.9 \text{ k}\Omega$. This value is lower than the value of $492 \text{ k}\Omega$ of the heterojunctions prepared by the sol-gel method⁽³⁴⁾.

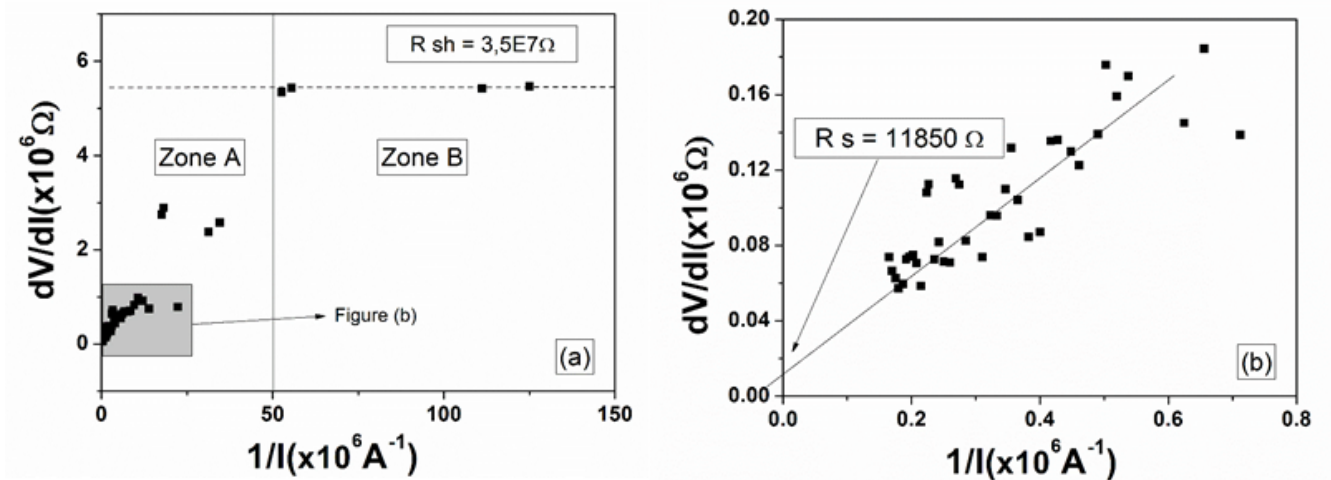


Fig 7. (a) dV/dI versus $1/I$, (b) dV/dI versus $1/I$ in the zone A.

The other two parameters, I_{sat} and n are obtained from the diode equation (11) after suppressing the effects of R_s and R_{sh} . Indeed, in the region where the exponential term in equation 11 is much higher than 1, the current I_d flowing through the diode only is then:

$$\ln(I_d) = \ln(I_{sat}) + \beta y \tag{11}$$

where $y = V - R_s I$ and $I_d = I - \frac{y}{R_{sh}}$

Figure 8 shows the curve of $\ln(I_d) = f(y)$ and $\ln(I) = f(y)$. As it can be seen, both curves coincide in the high voltage region and present the same slope (β) which leads to an ideality factor of $n = 10$. The intercept of this linear part with the y-axis gives the value of $I_{sat} = 1.9 \times 10^{-7} \text{ A}$.

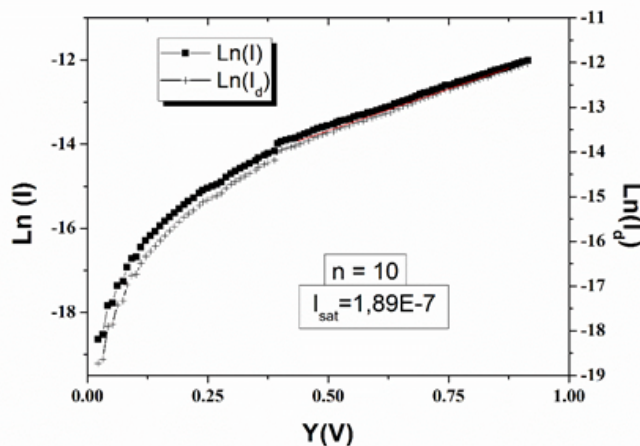


Fig 8. Plots of $\ln(I_d)$ and $\ln(I)$ versus y .

Compared to the literature results, the ideality factor n that we obtained has a value between $13^{(55)}$ and $6.8^{(57)}$, while it is lower than the value of 40.3 obtained by Prabu et al.⁽³⁴⁾. The departure of n from the ideal value of 1 is usually attributed to the recombination of electrons and holes in the depletion region and the interface between the two oxides. In this interface, there

is a high density of defects which is expected as a result of the large lattice mismatch between ZnO and CuO (on the order of 32%). Other conduction mechanisms such as space-charge-limited currents in the high voltage region⁽⁵⁵⁾ are not ruled out. In addition, the formation of an interfacial aluminum oxide layer between the Al electrodes and CuO may also lead to non-ideal diode behavior.

Also, it should be noted that the obtained shunt resistance is very high compared to the series resistance, which justifies the assumption made in the above method. In addition, this large value of R_{sh} suggests that there is no low-resistance paths (short-circuits) in the junction which confirms the good quality of the deposited thin films. Moreover, the high series resistance of the structure ($R_s = 11.9 \text{ k}\Omega$) may be due to the high resistivity of the CuO thin films as result of the low carrier mobility (mobility of holes in CuO $\leq 1 \text{ cm}^2 \text{ V}^{-1} \text{ s}^{-1}$ ⁽⁵⁸⁾) and the low doping levels. The contact resistance as well as the formation of an oxide layer on the Al electrode may also contribute to the series resistance.

In order to obtain further information about the junction properties, the capacitance-voltage (C-V) and the conductance-voltage (G-V) characteristics of the heterojunction were measured at 1 kHz in the DC bias voltage range $\pm 2 \text{ V}$. For a one-sided pn junction (heterojunctions) and in the depletion approximation, the capacitance per unit area is given by:

$$\frac{1}{C^2} = \left(\frac{2}{qN_a \epsilon_0 \epsilon'} \right) \left(V - V_{bi} - \frac{kT}{q} \right) \tag{12}$$

where V is the applied reverse bias voltage, V_{bi} is the built-in voltage (diffusion potential), ϵ' is the relative dielectric constant (equal to 2.4⁽⁵⁹⁾) and N_a is the effective doping density. T , q , ϵ_0 , and k represent respectively the measurement temperature, electron charge, vacuum permittivity and Boltzmann's constant⁽⁶⁰⁾. It is assumed that the doping level of ZnO:Al is much higher than that of CuO and therefore the depletion region extends mainly in the CuO film.

As it can be observed in Figure 9 (a), a linear region can be clearly seen in the plot of C^{-2} vs V in the reverse bias-region which suggests the existence of a depletion region within the structure. The intercept of this linear fit with the voltage axis yields the value of the built-in potential V_{bi} , while its slope gives the doping level according to equation (15).

From this plot, a value of 1.5 V is obtained for V_{bi} , which is close to the value of 1.55 V obtained for CuO/ZnO thin film heterojunctions reported by other works⁽⁵⁵⁾. Indeed, the diffusion potential is the difference between the work function of CuO ($\geq 5.8 \text{ eV}$) and that of ZnO ($\geq 4.2 \text{ eV}$) and is expected to be on the order of 1.4 eV. The differences between the obtained experimental and the theoretical values are attributed to the fact that the work functions are surface properties which are affected by the state of the surface as well as the interface between the two oxides. The doping level obtained from the slope of the line fit is $N_a = 1.1 \times 10^{17} \text{ cm}^{-3}$ which is in close agreement with values reported for CuO prepared by RF-sputtering⁽⁶¹⁾. This doping level and the low mobility of holes in CuO further support the values of the series resistance of the heterojunctions.

Moreover, the asymmetric nature of the conductance voltage characteristic, shown in Figure 9-b, further confirms the rectifying nature of the present heterojunction.

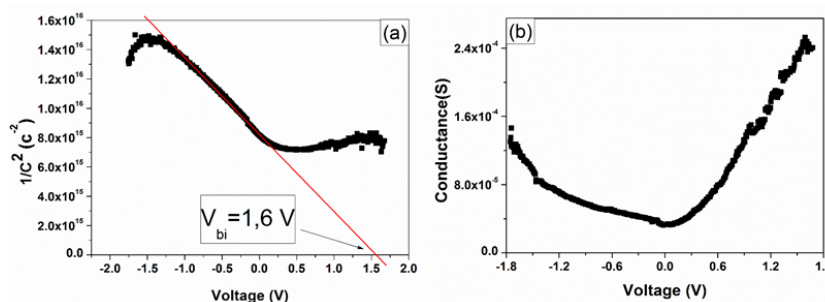


Fig 9. (a) The capacitance-voltage (C-2-V) and (b) The conductance-voltage (G-V) characteristics of the CuO/ZnO:Al heterojunction.

4 Conclusion

ITO/ ZnO:Al(1%)/CuO/Al heterojunction was successfully fabricated by combining thin films deposited by RF-sputtering and spin coating. The as-deposited films were polycrystalline. The optical band gap of the obtained CuO and ZnO films are found to be 1.58 and 3.27 eV respectively. The prepared thin films are in good quality in terms of the purity and surface uniformity. On the other hand, the prepared heterojunction showed a rectifying behavior and the I-V characteristics were analyzed in terms of the modified Shockley diode equation model. The analysis yielded to a shunt resistance of $3.5 \times 10^7 \Omega$, a series resistance of

11.9 k Ω , an ideality factor of 10 and a saturation current of about 1.9×10^{-7} A. Furthermore, the capacitance-voltage and the conductance-voltage measurements confirm the rectifying nature of the junction with a V_{bi} of 1.6 V.

References

- 1) Oral AY, Menşur E, Aslan MH, Başaran E. The preparation of copper(II) oxide thin films and the study of their microstructures and optical properties. *Materials Chemistry and Physics*. 2004;83(1):140–144. Available from: <https://dx.doi.org/10.1016/j.matchemphys.2003.09.015>.
- 2) Poloju M, Jayababu N, Reddy MVR. Improved gas sensing performance of Al doped ZnO/CuO nanocomposite based ammonia gas sensor. *Materials Science and Engineering: B*. 2018;227:61–67. Available from: <https://dx.doi.org/10.1016/j.mseb.2017.10.012>.
- 3) Ishizuka S, Kato S, Maruyama T, Akimoto K. Nitrogen Doping into Cu₂O Thin Films Deposited by Reactive Radio-Frequency Magnetron Sputtering. *Japanese Journal of Applied Physics*. 2001;40(Part 1, No. 4B):2765–2768. Available from: <https://dx.doi.org/10.1143/jjap.40.2765>.
- 4) Jeong S, Aydil ES. Heteroepitaxial growth of Cu₂O thin film on ZnO by metal organic chemical vapor deposition. *Journal of Crystal Growth*. 2009;311(17):4188–4192. Available from: <https://dx.doi.org/10.1016/j.jcrysgro.2009.07.020>.
- 5) Mukhopadhyay AK, Chakraborty AK, Chatterjee AP, Lahiri SK. Galvanostatic deposition and electrical characterization of cuprous oxide thin films. *Thin Solid Films*. 1992;209(1):92–96. Available from: [https://dx.doi.org/10.1016/0040-6090\(92\)90015-4](https://dx.doi.org/10.1016/0040-6090(92)90015-4).
- 6) Nakaoka K, Ogura K. Electrochemical Preparation of p-Type Cupric and Cuprous Oxides on Platinum and Gold Substrates from Copper(II) Solutions with Various Amino Acids. *Journal of The Electrochemical Society*. 2002;149(11):C579–C579. Available from: <https://dx.doi.org/10.1149/1.1512670>.
- 7) Baik DG, Cho SM. Application of sol-gel derived films for ZnO/n-Si junction solar cells. *Thin Solid Films*. 1999;354(1-2):227–231. Available from: [https://dx.doi.org/10.1016/S0040-6090\(99\)00559-3](https://dx.doi.org/10.1016/S0040-6090(99)00559-3).
- 8) Zhang P, Hong RY, Chen Q, Feng WG. On the electrical conductivity and photocatalytic activity of aluminum-doped zinc oxide. *Powder Technology*. 2014;253:360–367. Available from: <https://dx.doi.org/10.1016/j.powtec.2013.12.001>.
- 9) Rühle S, Anderson AY, Barad HN, Kupfer B, Bouhadana Y, Rosh-Hodosh E, et al. All-Oxide Photovoltaics. *The Journal of Physical Chemistry Letters*. 2012;3(24):3755–3764. Available from: <https://dx.doi.org/10.1021/jz3017039>.
- 10) Shiu HY, Tsai CM, Chen SY, Yew TR. Tri-Rung Yew. Solution-processed all-oxide nanostructures for heterojunction solar cells. *J Mater Chem*. 2011;21. Available from: <https://doi.org/10.1039/c1jm13303a>.
- 11) AitDads H, Bouzit S, Nkhaili I, Elkissani A, Outzourhit A. Structural, optical and electrical properties of planar mixed perovskite halides/Al-doped Zinc oxide solar cells. *Solar Energy Materials and Solar Cells*. 2016;148:30–33. Available from: <https://dx.doi.org/10.1016/j.solmat.2015.09.063>.
- 12) Bae HY, Choi GM. Electrical and reducing gas sensing properties of ZnO and ZnO - CuO thin films fabricated by spin coating method. *Sensors and Actuators B*. 1999;55:47–54. Available from: [https://doi.org/10.1016/S0925-4005\(99\)00038-6](https://doi.org/10.1016/S0925-4005(99)00038-6).
- 13) Ye ZZ, Yang F, Lu YF, Zhi MJ, Tang HP, Zhu LP. ZnO nanorods with different morphologies and their field emission properties. *Solid State Communications*. 2007;142:425–433. Available from: <https://doi.org/10.1016/j.ssc.2007.03.037>.
- 14) Granqvist CG. Transparent conductors as solar energy materials: A panoramic review. *Solar Energy Materials and Solar Cells*. 2007;91(17):1529–1598. Available from: <https://dx.doi.org/10.1016/j.solmat.2007.04.031>.
- 15) Gordon RG. Criteria for Choosing Transparent Conductors. *MRS bulletin*. 2000;p. 52–57. Available from: <https://doi.org/10.1557/mrs2000.151>.
- 16) Ginley DS, Bright C. Transparent Conducting Oxides. *MRS Bulletin*. 2000;25(8):15–18. Available from: <https://dx.doi.org/10.1557/mrs2000.256>.
- 17) Fortunato E, Brida D, Ferreira I, Águas H, Nunes P, Martins R. Production and characterization of large area flexible thin film position sensitive detectors. *Thin Solid Films*. 2001;383(1-2):310–313. Available from: [https://dx.doi.org/10.1016/S0040-6090\(00\)01610-2](https://dx.doi.org/10.1016/S0040-6090(00)01610-2).
- 18) Chopra KL, Major S, Pandya DK. Transparent conductors—A status review. *Thin Solid Films*. 1983;102:1–46. Available from: [https://dx.doi.org/10.1016/0040-6090\(83\)90256-0](https://dx.doi.org/10.1016/0040-6090(83)90256-0).
- 19) Lehraki N, Aida MS, Abed S, Attaf N, Attaf A, Poulain M. ZnO thin films deposition by spray pyrolysis: Influence of precursor solution properties. *Current Applied Physics*. 2012;12(5):1283–1287. Available from: <https://dx.doi.org/10.1016/j.cap.2012.03.012>.
- 20) Chen Z, Shum K, Salagaj T, Zhang W, Strobl K. ZnO Thin Films Synthesized by Chemical Vapor Deposition. In: Applications and Technology Conference. 2010;p. 4–9.
- 21) Znaidi L, Chauveau T, Tallaire A, Liu F, Rahmani M, Bockelee V, et al. Textured ZnO thin films by sol–gel process: Synthesis and characterizations. *Thin Solid Films*. 2016;617(b):156–160. Available from: <https://dx.doi.org/10.1016/j.tsf.2015.12.031>.
- 22) Tsoutsouva MG, Panagopoulos CN, Papadimitriou D, Fasaki I, Kompitsas M. ZnO thin films prepared by pulsed laser deposition. *Materials Science and Engineering: B*. 2011;176(6):480–483. Available from: <https://dx.doi.org/10.1016/j.mseb.2010.03.059>.
- 23) Olvera MDL, Maldonado A, Asomoza R. ZnO : F thin films deposited by chemical spray : effect of the fluorine concentration in the starting solution. *Solar Energy Mater Sol Cells*. 2002;73:425–433. Available from: [https://doi.org/https://doi.org/10.1016/S0927-0248\(02\)00211-8](https://doi.org/https://doi.org/10.1016/S0927-0248(02)00211-8).
- 24) Shishodia PK, Kim HJ, Wakahara A, Yoshida A, Shishodia G, Mehra RM. Plasma enhanced chemical vapor deposition of ZnO thin films. *Journal of Non-Crystalline Solids*. 2006;352(23-25):2343–2346. Available from: <https://dx.doi.org/10.1016/j.jnoncrysol.2006.01.086>.
- 25) Gao W, Li Z. ZnO thin films produced by magnetron sputtering. *Ceramics International*. 2004;30(7):1155–1159. Available from: <https://dx.doi.org/10.1016/j.ceramint.2003.12.197>.
- 26) Yang P, Wen H, Jian S, Lai Y, Wu S, Chen R. Characteristics of ZnO thin films prepared by radio frequency magnetron sputtering. *Microelectronics Reliability*. 2008;48(3):389–394. Available from: <https://doi.org/10.1016/j.microrel.2007.08.010>.
- 27) Nause J, Nemeth B. Pressurized melt growth of ZnO boules. *Semiconductor Science and Technology*. 2005;20(4):S45–S48. Available from: <https://dx.doi.org/10.1088/0268-1242/20/4/005>.
- 28) Afanasjev V, Bazhan M, Klimentov B, Mukhin N, Chigirev D. Thin-film heterostructures based on oxides of copper and zinc obtained by RF magnetron sputtering in one vacuum cycle. *Journal of Physics: Conference Series*. 2016;729(1):012013–012013. Available from: <https://dx.doi.org/10.1088/1742-6596/729/1/012013>.
- 29) Chatkaewsueb S, Saysunee N, Tamaekong N. The synthesis and characterization of p-CuO/n-ZnO nanoparticles synthesized by chemical method. *Materials Today: Proceedings*. 2017;4(5):6111–6117. Available from: <https://dx.doi.org/10.1016/j.matpr.2017.06.102>.
- 30) Ghosh A, Mondal A. Fabrication of stable, efficient and recyclable p-CuO / n-ZnO thin film heterojunction for visible light driven photocatalytic degradation of organic dyes. *Mater Lett*. 2016;164:221–224. Available from: <http://dx.doi.org/10.1016/j.matlet.2015.10.148>.
- 31) Terasako T, Murakami T, Hyoudou A, Shirakata S. Structural and electrical properties of CuO films and n-ZnO/p-CuO heterojunctions prepared by chemical bath deposition based technique. *Solar Energy Materials and Solar Cells*. 2015;132:74–79. Available from: <https://dx.doi.org/10.1016/j.solmat>.

2014.08.023.

- 32) Kumar GM, Ilanchezhyan P, Kumar AM, Shabi TS, Selvan ST, Suresh S, et al. Chemically-derived CuO/In₂O₃-based nanocomposite for diode applications. *CrystEngComm*. 2015;17(31):5932–5939. Available from: <https://dx.doi.org/10.1039/c5ce00853k>.
- 33) Hoppe M, Ababii N, Postica V, Lupan O, Polonskyi O, Schütt F, et al. CuO-Cu₂O / ZnO : Al heterojunctions for selective volatile organic compound detection. *Sensors Actuators B Chem*. 2018;255(2):1362–1375. Available from: <http://dx.doi.org/10.1016/j.snb.2017.08.135>.
- 34) Prabhu RR, Saritha AC, Shijeesh MR, Jayaraj MK. Fabrication of p-CuO/n-ZnO heterojunction diode via sol-gel spin coating technique. *Materials Science and Engineering: B*. 2017;220:82–90. Available from: <https://dx.doi.org/10.1016/j.mseb.2017.03.008>.
- 35) Nkhaili L, Elyaaougubi M, Elmansouri A, Khalfi AE, Elfathi A, Ali MA, et al. Optical, and Electrical Characteristics of Zinc Oxide and Copper Oxide Films and Their. *Spectroscopy Letters*. 2015;48(7). Available from: <https://doi.org/10.1080/00387010.2014.897732>.
- 36) Saji KJ, Populoh S, Tiwari AN, Romanyuk YE. Design of p-CuO/n-ZnO heterojunctions by rf magnetron sputtering. *physica status solidi (a)*. 2013;210(7):1386–1391. Available from: <https://dx.doi.org/10.1002/pssa.201228293>.
- 37) Drobný VF, Pulfrey L. Properties of reactively-sputtered copper oxide thin films. *Thin Solid Films*. 1979;61(1):89–98. Available from: [https://dx.doi.org/10.1016/0040-6090\(79\)90504-2](https://dx.doi.org/10.1016/0040-6090(79)90504-2).
- 38) Jannane T, Manoua M, Liba A, Fazouan N, Hichou E, Almagoussi A, et al. Sol-gel Aluminum-doped ZnO thin films: Synthesis and characterization. *Materials Environments Sciences*. 2017;8(1):160–168.
- 39) Morkoc H, Ozgur U. General Properties of ZnO. Zinc Oxide: Fundamentals, Materials and Device Technology. 2009.
- 40) Lauriat JP, Péro P. Adaption d'un ensemble de détection Si(Li) à un diffractometre X. *Journal of Applied Crystallography*. 1972;5:177–183. Available from: <https://dx.doi.org/10.1107/s002188987200915x>.
- 41) Prabhu YT, Rao KV, Kumar VSS, Kumari BS. X-Ray Analysis by Williamson-Hall and Size-Strain Plot Methods of ZnO Nanoparticles with Fuel Variation. *World Journal of Nano Science and Engineering*. 2014;04(01):21–28. Available from: <https://dx.doi.org/10.4236/wjnse.2014.41004>.
- 42) Chavan A, Shivraj BW, Murthy HNN, A V, Holla V, Shandilya S, et al. Parametric Study of Sol Gel Technique for Fabricating ZnO Thin Films. *Procedia Materials Science*. 2015;10:270–278. Available from: <https://dx.doi.org/10.1016/j.mspro.2015.06.050>.
- 43) Dimopoulos T, Peić A, Müllner P, Neuschitzer M, Resel R, Abermann S, et al. Photovoltaic properties of thin film heterojunctions with cupric oxide absorber. *Journal of Renewable and Sustainable Energy*. 2013;5(1):011205–011205. Available from: <https://dx.doi.org/10.1063/1.4791779>.
- 44) Janotti A, de Walle CGV. Fundamentals of zinc oxide as a semiconductor. *Reports on Progress in Physics*. 2009;72(12):126501–126501. Available from: <https://dx.doi.org/10.1088/0034-4885/72/12/126501>.
- 45) Laaziz Y, Bennouna A, Chabboun N, Outzourhit A, Ameziane EL. Optical characterization of low optical thickness thin films from transmittance and back reflectance measurements. *Thin Solid Films*. 2000;372(1-2):149–155. Available from: [https://dx.doi.org/10.1016/s0040-6090\(00\)00997-4](https://dx.doi.org/10.1016/s0040-6090(00)00997-4).
- 46) Jeong SH, Lee JW, Lee SB, Boo JH. Deposition of aluminum-doped zinc oxide films by RF magnetron sputtering and study of their structural, electrical and optical properties. *Thin Solid Films*. 2003;435:78–82. Available from: <https://doi.org/10.1016/S0040-6090>.
- 47) Musat V, Teixeira B, Fortunato E, Monteiro RCC, Vilarinho P. Al-doped ZnO thin films by sol-gel method. *Surface and Coatings Technology*. 2004;180-181:659–662. Available from: <https://dx.doi.org/10.1016/j.surfcoat.2003.10.112>.
- 48) Pavan M, Rühle S, Ginsburg A, Keller DA, Barad HN, Sberna PM, et al. TiO₂/Cu₂O all-oxide heterojunction solar cells produced by spray pyrolysis. *Solar Energy Materials and Solar Cells*. 2015;132:549–556. Available from: <https://dx.doi.org/10.1016/j.solmat.2014.10.005>.
- 49) Shaaban ER, Yahia IS, El-Metwally EG. Validity of Swanepoel's Method for Calculating the Optical Constants of Thick Films. *Acta Physica Polonica A*. 2012;121(3):628–635. Available from: <https://dx.doi.org/10.12693/aphyspola.121.628>.
- 50) Deepa K, Preetha KC, Murali KV, Dhanya AC, Ragina AJ, Remadevi TL. The effect of various complexing agents on the morphology and optoelectronic properties of chemically deposited ZnS thin films: A comparative study. *Optik*. 2014;125(19):5727–5732. Available from: <https://dx.doi.org/10.1016/j.ijleo.2014.06.028>.
- 51) Alsaad AM, Ahmad AA, Al-Bataineh QM, Bani-Salameh AA, Abdullah HS, Qattan IA, et al. Optical, Structural, and Crystal Defects Characterizations of Dip Synthesized (Fe-Ni) Co-Doped ZnO Thin Films. *Materials*. 2020;13(7):1737–1737. Available from: <https://dx.doi.org/10.3390/ma13071737>.
- 52) Alsaad AM, Ahmad AA, Qattan IA, Al-Bataineh QM, Albataineh Z. Structural, Optoelectrical, Linear, and Nonlinear Optical Characterizations of Dip-Synthesized Undoped ZnO and Group III Elements (B, Al, Ga, and In)-Doped ZnO Thin Films. *Crystals*. 2020;10(4):252–252. Available from: <https://dx.doi.org/10.3390/cryst10040252>.
- 53) Baydogan N, Ozdurmusoglu T, Cimenoglu H, Tugrul AB. Refractive Index and Extinction Coefficient of ZnO:Al Thin Films Derived by Sol-Gel Dip Coating Technique. *Defect and Diffusion Forum*. 2013;335:290–293. Available from: DOI:10.4028/www.scientific.net/DDF.334-335.290.
- 54) Ahmad AA, Alsaad AM, Al-Bataineh QM, Al-Naafa MA. Optical and structural investigations of dip-synthesized boron-doped ZnO-seeded platforms for ZnO nanostructures. *Applied Physics A*. 2018;124(6). Available from: <https://dx.doi.org/10.1007/s00339-018-1875-z>.
- 55) Hussain S, Cao C, Nabi G, Khan WS, Tahir M, Tanveer M, et al. Optical and electrical characterization of ZnO/CuO heterojunction solar cells. *Optik*. 2017;130:372–377. Available from: <https://dx.doi.org/10.1016/j.ijleo.2016.10.099>.
- 56) William S. Electrons and Holes in Semiconductors with applications to transistor electronics. D. Van nortrand vompany, inc. 1950.
- 57) Zainelabdin A, Zaman S, Amin G, Nur O, Willander M. Optical and current transport properties of CuO/ZnO nanocoral p-n heterostructure hydrothermally synthesized at low temperature. *Applied Physics A*. 2012;108(4):921–928. Available from: <https://dx.doi.org/10.1007/s00339-012-6995-2>.
- 58) Samokhvalov AA, Vigin NA, Gizhevskii BA, Loshkarev NN, Osipov VV, Solin LI, et al. Low-mobility charge carriers in CuO. *Experimental and Theoretical Physics*. 1993;103(3):951–961.
- 59) Ekuma CE, Anisimov VI, Moreno J, Jarrell M. Electronic structure and spectra of CuO. *The European Physical Journal B*. 2014;87(1):23–23. Available from: <https://dx.doi.org/10.1140/epjb/e2013-40949-5>.
- 60) Pukird S, Song W, Noothongkaew S, Kim SK, Min BK, Kim SJ, et al. Synthesis and electrical characterization of vertically-aligned ZnO-CuO hybrid nanowire p-n junctions. *Applied Surface Science*. 2015;351:546–549. Available from: <https://dx.doi.org/10.1016/j.apsusc.2015.05.164>.
- 61) Patel M, Kim HS, Kim J, Yun JH, Kim SJ, Choi EH, et al. Excitonic metal oxide heterojunction (NiO/ZnO) solar cells for all-transparent module integration. *Solar Energy Materials and Solar Cells*. 2017;170:246–253. Available from: <https://dx.doi.org/10.1016/j.solmat.2017.06.006>.